[1]R. Madhana
[2]Geetha Mani

A Novel Assimilate Power Flow Control Technique Based Multiport Converter For Hybrid Power Generation System With Grid-Connected Application

Journal of Electrical Systems

Abstract: Clean, sufficient energy from renewable resources such as the Sun, Wind, and other natural resources is provided via renewable energy technology. Electricity failure also increases with the electricity demand. Thus, consistent loads may be provided by renewable energy sources. A multiport conversion architecture has been developed for hybrid energy sources such as wind and solar sources. A practical method of producing power is to combine wind and sun resources. This study presents a coordinated control method and dynamic modelling tools for an integrated microgrid scheme that combines fuel cell technology, backup diesel generation, photovoltaic systems, battery generators, and assimilated power flow control (APFC). A unique vibrant filter compensator based on dynamics is employed to achieve a fully balanced integrated system. This ensures minimal inrush current, load excursions, and regulated DC bus voltage while optimizing the utilization of the diesel generator set. Our primary area is to achieve the most efficient operation of the integrated renewable energy sources, including PV panels and fuel cells. Photovoltaic Power System with Backup Fuel Cell Source for Hybrid Power System: The control unit in this hybrid system manages the power from both the fuel and the PV cells. When the control power is activated, it triggers the fuel cell and photovoltaic cell powers. The control device first checks if the photovoltaic cell is generating power. If the PV energy is sufficient to meet the load requirements, the control power links the photovoltaic energy to the load. In cases where the load cannot be fulfilled by photovoltaic power alone, the control system disconnects the photovoltaic cell power and switches to the backup fuel cell power. Afterwards, when the power generated from the photovoltaic cells reaches a sufficient level, the control system promptly switches from the fuel cell to the photovoltaic cells. The fuel cell is integrated with a photovoltaic system and a DC-DC boost conversion in conjunction with the resistive workload. The controller outputs have been fine-tuned, and PWM is generated and subsequently supplied to the converter's switching. The converter's design considers conversion efficiency, power sharing, system stability, and responsiveness in various operational scenarios to ensure successful operation. The effectiveness of the simulated output APFC techniques is evaluated for each parameter, such as steady-state error, THD, and the system's efficiency.

Keywords: Multiport Converter (MPC), Renewable energy generation, Assimilate Power Flow Control (APFC), zero steady-state error.

I. INTRODUCTION

A two-stage energy conversion system is shown in Figure 1. It consists of an inverter for energy conversion and a multiport isolation type DC-DC converter. Numerous sources, including fuel cells, wind turbine generators, and solar panels, are linked to the isolated DC-DC converter. The DC-DC converter is adjusted by the low-level DC voltage source inverter to keep the high level constant. Finally, for grid-connected applications, the stabilized DC output is converted to AC.

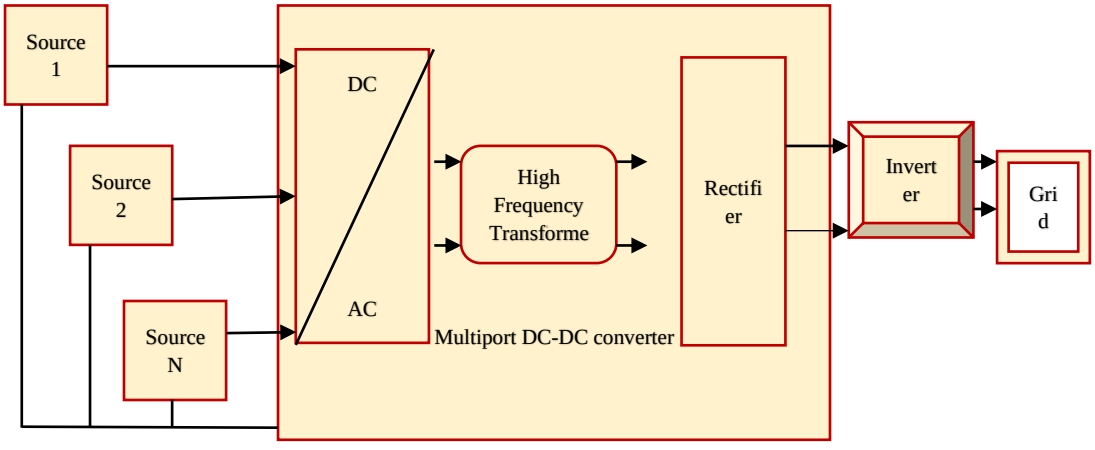

Fig1: Functional block diagram for the multiport DC-DC converter

[1]*Corresponding author: [1]Research Scholar, Vellore Institute of Technology, Vellore, 632014, India
[2]Professor, Vellore Institute of Technology, Vellore, 632014, India
madhanaeee@gmail.com[1], geetha.mani@vit.ac.in[2]
Correspondence Mail; madhanaeee@gmail.com

Two types of distinct integrated MPCs are used in the modern power system. One category of converters uses transformers for isolation and high-energy conversion purposes, and another one is without a transformer for low-power applications. In the proposed method, a transformer-based MPC converter is designed for the isolation circuit's high power application to protect the source system from sudden power feedback from the grid system. Advanced multiport converters reduce the number of switches in the course, minimizing the switching losses. A separate full-wave rectifier uses each port of two buttons. Recently, new multiport converter topologies have been proposed for RES systems like solar, Wind and battery-based energy management, which requires the power switch M + 1, where m is the source. The different output load regulations while maintaining high power transmission efficiency and reliability of flow control to use Assimilate Power Flow Control (APFC) control scheme art control schemes simple and reliable flow control. The topology of the hybrid energy storage system proposes low-power applications. New topology can absorb more renewable energy sources and various output power load levels. Thus, the controller circuit automatically adjusts the duty cycle value despite all source output voltage and load changes to obtain the desired constant output voltage.

This research presents a novel and flexible micro-network-based interconnect architecture. This paper presents the study and fundamental construction of the recently proposed MPC. This converter has two input ports that can connect two renewable energy sources to the load either simultaneously or independently, a two-way port that controls backup and store power, and an output port that is completely regulated.

II. LITERATURE SURVEY

For the performance improvement of the proposed MPC system, the drawbacks in the existing MPC system need to be identified using it in the existing MPC system using various techniques, which are discussed below.

A multiport DC-DC converter can transfer power between two DC and AC systems within a single converter structure. This feature can decrease the energy conversion rate [1]. This system offers a fault-tolerant topology for MPC cascaded DC/DC converters in solar power generation systems, meeting fault tolerance criteria [2]. This system aims to design and analyze a proposed MPC-based DC-DC buck-boost converter for high boost/buck applications [3]. This work utilizes a high-gain MPC in a hybrid energy storage system that combines low-voltage batteries and supercapacitors [4-9]. A non-isolated high pulse multi-terminal conversion with smooth switching is suggested, providing an independent power flow line between the input and output source.

A generator can be used as a power source to charge storage devices. In hybrid power applications, the DC bus output is an excellent choice for the converter [10-11]. For independent PV systems, a non-isolated Switched-Capacitor Converter (SCC) Series (SC-MPC) is recommended to reduce the converter's size while maintaining effective operation [12]. The proposed architecture reduces overall cost, size, weight, and complexity by using fewer components to achieve the same voltage increase. Despite its high voltage gain, the peak reverse voltage of the diode's return switch is minimal [13-15]. The suggested topology for the DC link (MPC) is based on two parallel DC-DC power electronic converters with independent input and output. In the two stages of energy conversion in the DC system, the initial boost converter is used for energy enhancement, whereas the fly-back converter is used for energy stabilization with a lower ripple ratio [16]. The Single Input Dual Output (SIDO)-TLC is a three-stage step-down/step-up converter with synchronous output voltage regulation. This new topology offers several key advantages, including lower voltage stress across semiconductor devices, greater efficiency, and reduced inductance [17-18]. A center-tap transformer was used to facilitate the connection between two separate DC sources and loads [19]. The steady-state operation analysis and control technique of the proposed topology applies to converters in both buck and boost configurations. A general method is used to analyze the proposed closed-loop system, and case studies demonstrated the local stability of the automatic traction of the three-stage MIMO-MMC over a wide range of operating points [20-28].

III. PROPOSED SYSTEM

The proposed optimization model optimizes the load according to its priority level and energy availability. Keeping the DC bus stable under any source-side fluctuation is also recommended. Figure 2 Displays the system setup for the proposed hybrid energy system stabilized by PV, Wind and battery-based energy stabilization.

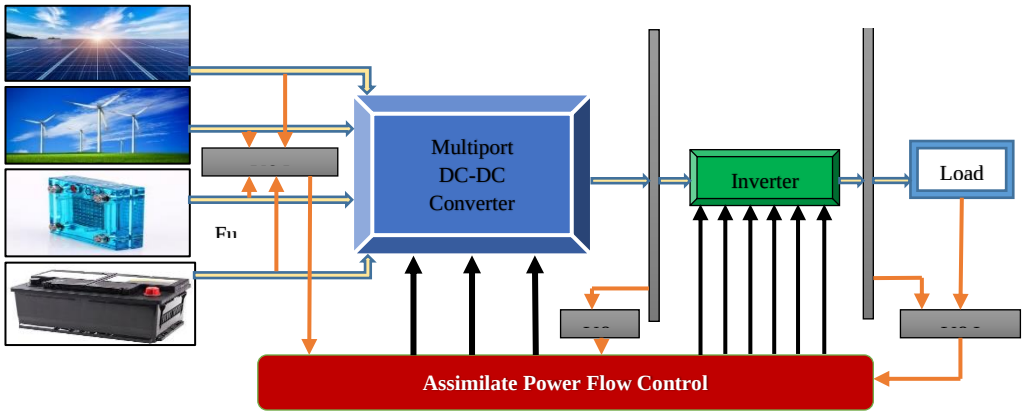

Fig. 2: Proposed multiport converter using Assimilate Power Flow Control

A Solar Power Generation

The radiant light and heat of the Sun that are caught by a range of constantly evolving technologies is known as photovoltaic energy. Examples of these technologies include artificial photosynthesis, salt-based power plants, photovoltaic heating, and photovoltaic and warmth from the Sun. It is a substantial renewable energy source, and the ways in which it collects, distributes, or converts photovoltaic energy into photovoltaic power are referred to as either passive or active photovoltaic technologies. Employing solar panels, concentrated photovoltaic electricity, and photovoltaic water heating are examples of active photovoltaic resource harvesting techniques.

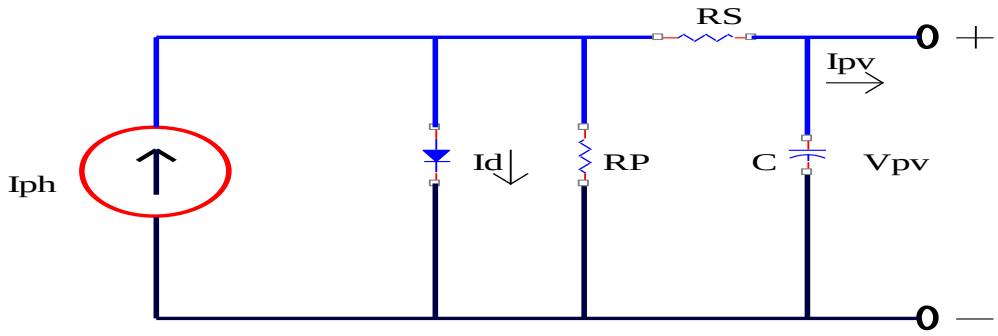

Fig. 3: An identical circuit for a separate photocell

Figure 3 shows the single diode-based equivalent circuit. This mode provides a good balance between precision and simplicity. The photocurrent is generated by the module and diode current, respectively. The comparable series and parallel resistance of the module. In the case of a series connection and several PV modules arranged in parallel, a parasitic capacitance will be modelled as a capacitor in the model shown in Figure 3. The voltage-current characteristics of a PV module-based expression are described below;

$$I_{PV}(t) = I_{Ph}(t) - I_0(t)\left[\exp\left(\frac{V_{PV}(t)+R_s I_{PV}(t)}{n_d N_s}\frac{q}{kT_c(t)}\right) - 1\right] - \frac{V_{PV}(t)+R_s I_{PV}(t)}{R_P} \quad (1)$$

$$I_{Ph}(t) = I_{Ph,stc} + K_i \Delta T_c(t))\frac{S_x(t)}{S_{stc}} \quad (2)$$

$$I_{Ph,stc} = \frac{R_P+R_s}{R_P} I_{sc,stc} \quad (3)$$

$$I_0(t) = \frac{I_{SC,stc}+K_i \Delta T_c(t)}{\left[\exp\left(\frac{V_{OC,stc}+K_V \Delta T_c(t)}{n_d N_s}\frac{q}{kT_c(t)}\right)-1\right]} \quad (4)$$

The representation of the above symbols is given below;

q=The electron charge ($1.602x10^{-19}$ C)

n_d= diode ideally factor (-)

K=The Boltzmann constant ($1.38x10^{-23}$ J/k)

I_0 = Reverse saturation current of the diode at cell temperature T_x(A)

I_d = The diode current (A)

$I_{Ph,stc}$ =Photocurrent at STC (A)

I_{Ph} = photocurrent at cell temperature and solar irradiance (A)

$I_{SC,stc}$ = Short circuit current (A)

K_i = Factors in the change in the slope of the photocurrent variations due to the temperature of the battery (-)

B Wind Power Generation

Pressure differences induce air movement, which gives rise to wind. It moves from high-pressure zones to low-pressure zones. Higher air pressure gradients result in higher wind speeds, which raises the amount of wind power that can be captured by wind energy conversion technologies. The link between WPF and the grid and electricity generation is depicted in Figure 4. The wind turbine employed in this review has the following output characteristics (PWT is the wind speed):

Power is supplied by the wind generated by the wind = (air density * sweep area * cube of velocity) / 2

$$p_w = \frac{1}{2(A_w)(v)^3} \cdots \quad (5)$$

Where,

P = power in watts (W)

ρ = Wind-Air density in (kg/m³)

A_w = Swept area by air (m²)

V = Wind velocity in (m/s).

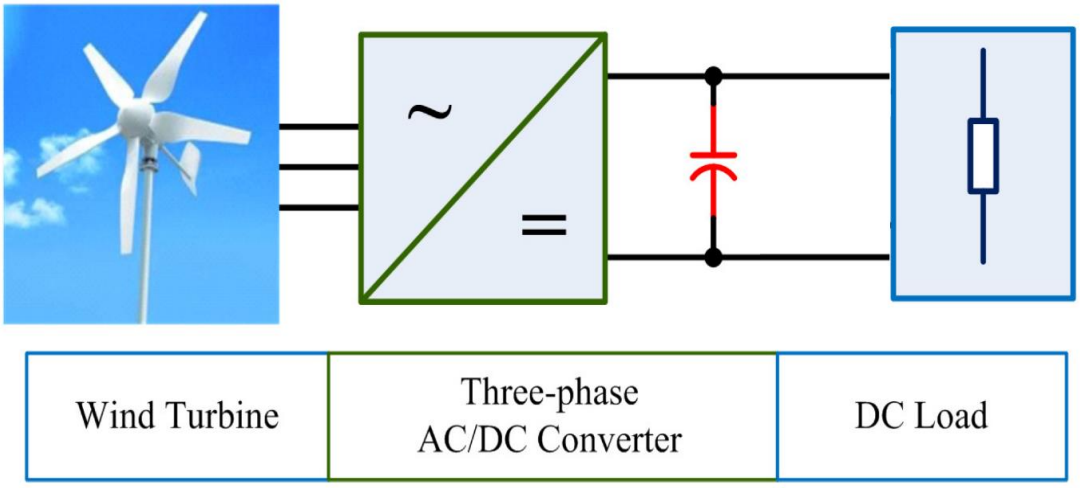

Fig. 4: Block for Wind energy system

Equation 6 states the power density, also known as specific power, based on the air density and wind speed at a given place,

$$\frac{P}{A} = \frac{1}{2}\rho v^3 \quad \cdots \quad (6)$$

The system's overall power can be deemed equivalent to the power compensated by the converter for the improved power supply. The electricity generation of the wind energy can be expressed in numerical terms as outlined below;

$$P_T = N_w * P_w \quad \cdots \quad (7)$$

Where,

P_T= Total energy produced

P_w = power generated by wind turbines

N_w= No of wind turbine

C Fuel cell energy generation

Fuel cells, essentially batteries that never run out as long as there is a continuous supply of oxygen and hydrogen, are highly suited for distributed power generation applications. Hydrogen can be obtained directly or indirectly through reformers, which manufacture it from gasoline, natural gas, and alcohol.

Phosphoric acid fuel cells are commercially available in the 200 kW range, although solid oxide and molten carbonate fuel cells are still in the pre-commercial study stage. Because gasoline may be used as fuel for fuel cell technologies, a lot of development work has been done. The output voltage, modelled based on the design of the fuel cell equivalent circuit, is shown in Figure 5

The Equivalent Circuit of the fuel cell

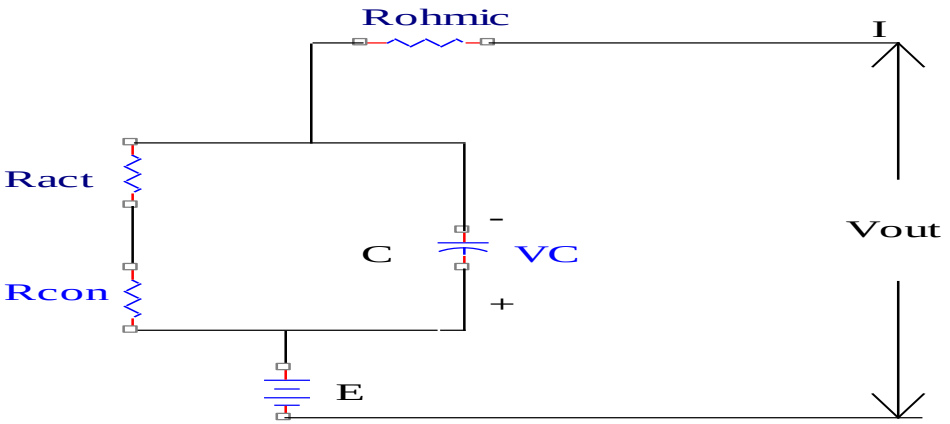

Fig. 5: Equivalent circuit of fuel cell

$$V_{cell} = E_{cell}\_V_{act} - V_{ohm,} - V_{conc}, Cell \quad \ldots \quad (8)$$

The output voltage that can be obtained is represented below;

$$V_{out} = Ncell.Vcell = E - V_{act} - V_{ohm,} - V_{conc} \quad \ldots \quad (9)$$

Where V_{cell} =fuel cell voltage.

E_{cell}=reversible potential

V_{act} =Activation voltage loss

D Battery modeling

The optimal battery modelling is based on the operation of the proposed MPC converter. The battery is in charging mode whenever renewable energy is sufficient to generate power to meet the required load demand. If RES cannot meet the load, the battery is in discharging mode. The following formula calculates this:

$$B_a(t) = B_a(t-1) + ((B_s(T\text{-}1) + B_t(t-1).C_{bat} \quad \ldots \quad (10)$$

Where $B_a(t)$ is a rechargeable battery at time t, $B_a(t-1))$ at the time of charging the battery T-1, $B_s(t-1)$ will be stored at time t-1, and the charge amount of the P (t- 1) is the total energy provided by the battery at the time t, C_{bat}bat battery charging efficiency.

A state of charge (SOC) depending on the load requirements and the state of the power supplied by the RES and is calculated using the following formula:

In the charging state,

$$SOC(t) = SOC(t-1) + \frac{B_{bat(t)}B_{char}}{PN} \quad \ldots \quad (11)$$

During the discharging state,

$$SOC(t) = SOC(t-1) + \frac{B_{bat(t)}B_{dis}}{P_N}.100 \quad \ldots \quad (12)$$

Wherein the SOC (t) is the cell at time t the state, $B_{bat(t)}$ is the power exchanged during a time stepΔt, B_{char} battery charging efficiency, B_{dis} battery discharge efficiency, and P_N is the battery's nominal capacity of the battery

3.5 Design and implementation of the Proposed Multiport converter

Figure 6 illustrates a circuit diagram for an isolation transformer-based proposed MPC (Model Predictive Control) converter. The proposed converter offers dual energy conversion ranges: low- and high-voltage conversion. The high-frequency transformer is employed for high-voltage conversion, and its isolation feature protects the input source. The circuit includes a Low Voltage Switch (LVS) with an m parallel port, a power storage capacitor, and the primary winding of the transformer.

There is an inductor, diode, and power switch on each port. An HVS LC filter circuit and full-wave rectifier are coupled to the secondary winding of the transformer. The definition of the turns ratio transformation is n = NS / NP, where NP and NS stand for the primary and secondary winding turns, respectively. To ensure the proper operation of various sources, the following requirements must be met:

When d_1 = 1, 2... M turns off; it does so only if d_1 was previously closed; otherwise, the continuous energy of d_m is stored in the storage. Both d_2 and d_3 shouldn't be turned off at the same time. To meet this requirement, the converter must satisfy the following inequality.

$$\min(d_2, d_3 \ldots d_m) \geq d_1 \quad \ldots \quad (13)$$

Where $d_1 (i = 1 \ldots m)$ is the PWM of the switch S_1.

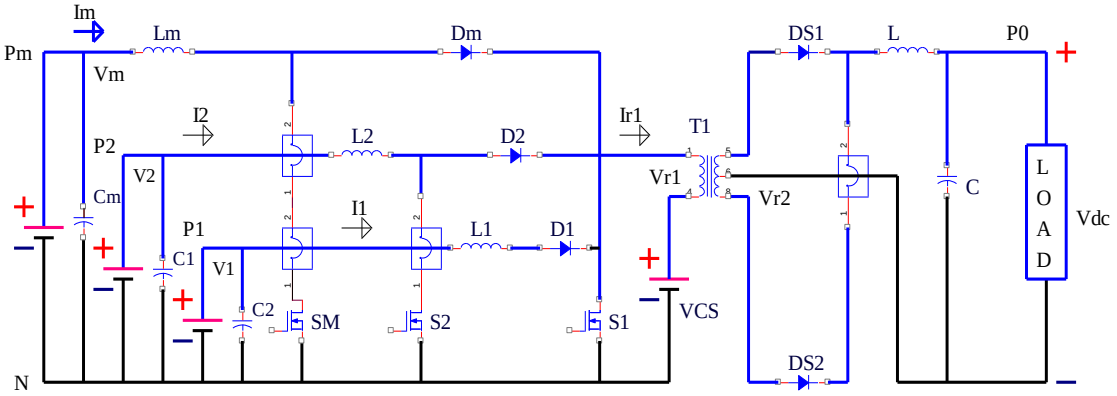

Fig. 6: Proposed multiport DC-DC converter circuit.

If the source voltage of port 1 (P_1) is the largest, that is, $V_1 \geq V_K$, where V_K is the k^{th} source (K=2... M), the rated output voltage of the inequality (1) is satisfied. There are three ways to use this converter: the state of all the switches, switches s_1, at least one other switch in the closed state is opened, and all controls are off. The equivalent circuit for a switching period of three operational modes is shown in Figure 7 in a switching cycle when m = 3. In the present specification, the three kinds of operation modes of the converter and the state-space equations are given below:

$$Q.x = A.x + B \quad \ldots \quad (14)$$

Where Q=diag (L_1, L_2 .... L_m, Cs, L, C);

$$x = [i_1, i_2 \ldots i_m, V_{Cs}, i_L, V_{dc}]^T \quad \ldots \quad (15)$$

Mode 1: $t \in [t_0, t_1]$ the working operation for mode-1; during this period, all switches are in conjunction with inductors L1... Lm to extract energy from the source. The energy stored in the capacitor C_s was previously exchanged, and the diode delivered the cycle to the HVS through D_{s1} and D_{s2}. During the mode-1 operation, all the switches are in the state; in that time, the source energy like solar (P_m), wind (P_2) and fuel cell (P_1) energy are connected to the load system, the battery (V_{cs}) is in charging state the energy flow diagram is represented in below figure7.

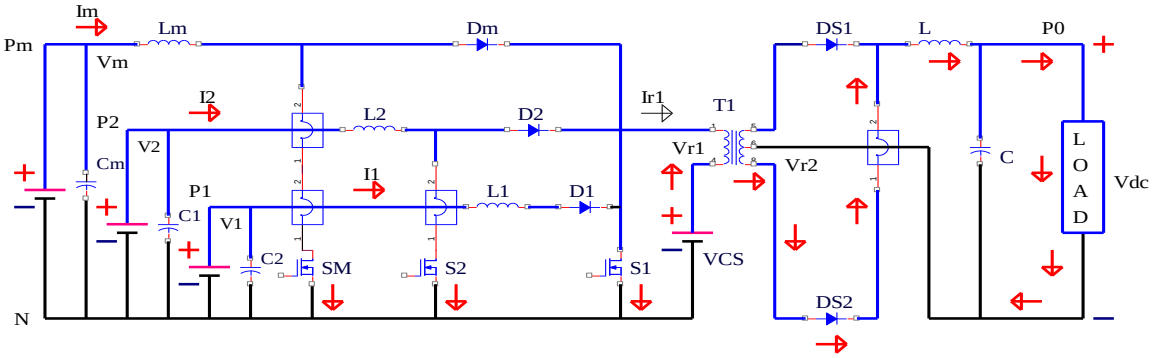

Fig. 7: Mode-1 operation for the proposed converter

The state-space equation is expressed below;

$$Q.x = \begin{bmatrix} 0 & 0 & \ldots & 0 & 0 & 0 & 0 \\ 0 & 0 & \ldots & 0 & 0 & 0 & 0 \\ \vdots & \vdots & \ddots & \vdots & \vdots & \vdots & \vdots \\ 0 & 0 & \ldots & 0 & 0 & 0 & 0 \\ 0 & 0 & \ldots & 0 & 0 & 0 & 0 \\ 0 & 0 & \ldots & 0 & n & 0 & -1 \\ 0 & 0 & \ldots & 0 & 0 & 1 & -1/R \end{bmatrix} .x + \begin{bmatrix} V_1 \\ V_2 \\ \vdots \\ V_m \\ -i_{cs} \\ 0 \\ 0 \end{bmatrix} \quad \ldots \quad (16)$$

Mode 2: When S1 is closed, at least one switch SK (K=2... m) is turned on. This pattern has $2^{(m-1)}-2$ depending on the switch S2 ... Sm in a state of two different schemes. An operation of mode two is shown in Figure 8 with the switching operation where only one controller is s_k, and all other switches are off. During the mode-2 process, only the SK (K=2, m) is in a state of stability; due to the stability of the power generation-based load-connected condition, the SK and SM are turned on/off. Figure 8 shows the solar (P_m) is high at that time, the wind (P_2) and fuel cell (P_1) energy are not connected to the load system, and the battery (V_{cs}) is the charging state energy flow diagram, which is represented in the figure below.

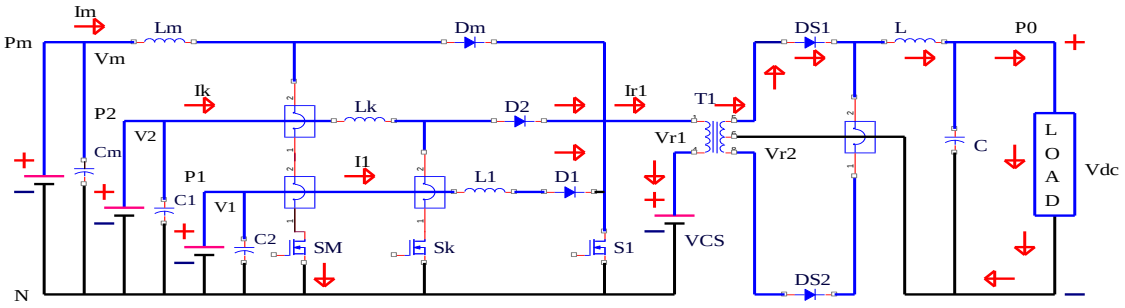

Fig. 8: Mode-2 operation for the proposed converter

The state-space equation is:

$$Q.x=\begin{bmatrix}0&\cdots&0&0&0&\cdots&0&-1&0&0\\ \vdots&\ddots&\vdots&\vdots&\vdots&\ddots&\vdots&\vdots&\vdots&\vdots\\ 0&\cdots&0&0&0&\cdots&0&-1&0&0\\ 0&\cdots&0&0&0&\cdots&0&-1&0&0\\ 0&\cdots&0&0&0&\cdots&0&0&0&0\\ \vdots&\ddots&\vdots&\vdots&\vdots&\ddots&\vdots&\vdots&\vdots&\vdots\\ 0&\cdots&0&0&0&\cdots&0&-1&0&0\\ 1&\cdots&1&0&1&0&1&0&0&0\\ 0&\cdots&0&0&0&\cdots&0&0&0&-1\\ 0&\cdots&0&0&0&\cdots&0&0&1&-1/R\end{bmatrix}.x+\begin{bmatrix}V_{1-}V_{r1}\\ \vdots\\ V_{k-1-}V_{r1}\\ V_K\\ V_{k-1-}V_{r1}\\ \vdots\\ V_m\\ 0\\ n.V_{r1}\\ 0\end{bmatrix} \quad \dots \quad (17)$$

Mode 3: $t \in [t_3, t_4]$ The working operation for mode-3, all switches are off during this period. Figure 9 determines the mode-3 function of the proposed MPC. During the mode-3 process, all the switches are turned off state, so the source energy, such as solar (P_m), wind (P_2) and fuel cell (P_1) energy are not connected to the load system because the switches are on state; the only battery (V_{cs}) sources are connected to the load system.

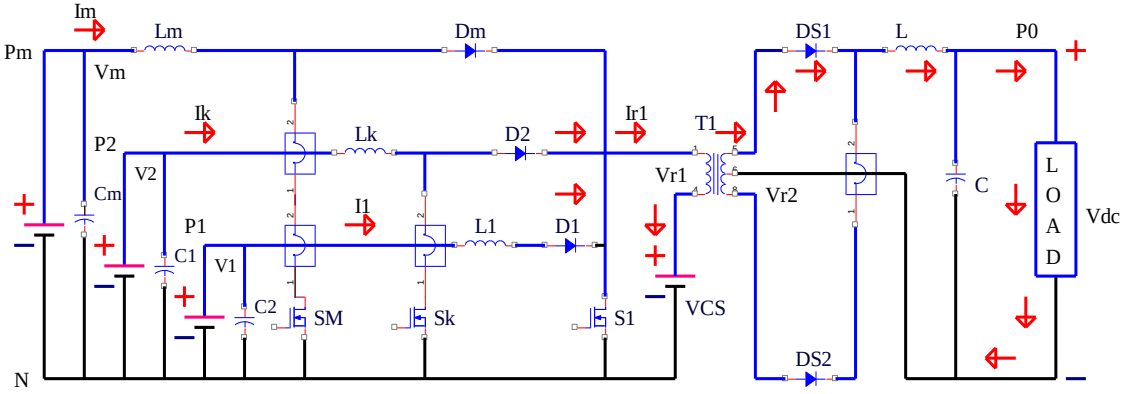

Fig. 9: Mode-3 operation of the proposed converter

The state-space equation is:

$$Q.x=\begin{bmatrix}0&0&\dots&0&-1&0&0\\ 0&0&\dots&0&-1&0&0\\ \vdots&\vdots&\ddots&\vdots&\vdots&\vdots&\vdots\\ 0&0&\dots&0&-1&0&0\\ 1&1&\dots&1&0&0&0\\ 0&0&\dots&0&0&0&-1\\ 0&0&\dots&0&0&1&-1/R\end{bmatrix}.x+\begin{bmatrix}V_{1-}V_{r1}\\ V_{2-1-}V_{r1}\\ \vdots\\ V_{m-}V_{r1}\\ 0\\ n.V_{r1}\\ 0\end{bmatrix} \quad \dots \quad (18)$$

Based on the (3)-(5), It is possible to express the average state-space model as;

$$Q.x = \begin{bmatrix} 0 & 0 & \dots & 0 & -(1-d_1) & 0 & 0 \\ 0 & 0 & \dots & 0 & -(1-d_2) & 0 & 0 \\ \vdots & \vdots & \ddots & \vdots & \vdots & \vdots & \vdots \\ 0 & 0 & \dots & 0 & -(1-d_m) & 0 & 0 \\ -(1-d_1) & -(1-d_2) & \dots & -(1-d_m) & 0 & 0 & 0 \\ 0 & 0 & \dots & 0 & nd1 & 0 & -1 \\ 0 & 0 & \dots & 0 & 0 & 1 & -1/R \end{bmatrix} .x + \begin{bmatrix} V_{1-} - (1-d_1)V_{r1} \\ V_{2-1-} - (1-d_2)V_{r1} \\ \vdots \\ V_{m-} - (1-d_m)V_{r1} \\ -d_1 i_{cs} \\ n.-(1-d_1)V_{r1} \\ 0 \end{bmatrix}$$

…

(19)

The balance point can be set through all (6), then the time derivative term is calculated as zero;

$$D_k = 1 - (1 - D_1).V_k/V_1 \qquad k=2\dots m \quad \dots \qquad (20)$$

$$I_{cs}.D_1 = \sum_{k=1}^{m} I_K(1 - D_k) \qquad (21)$$

Subsequently, the fixed voltage and sampling error voltage are considered for energy stabilization, defined in equation (20); during this condition, the D_k (k = 2... m) is maintained as constant. If (20) is unsatisfied, the input source will be modified based on the switching operation.

These issues are mainly caused by the parallel connection of sources coupled with a transformer. Due to these concerns, the proposed APFC controller will be decoupling the energy flow in each port. The energy is maintained constantly based on the time-based switching function. For example, port voltage and current should be controlled when d1 is an update D_k (k = 2, ⋯, m). The APFC strategy will be implemented by modifying the port's duty cycle based on the availability of input sources. Battery-based energy management will also provide a power source when RES does not provide sufficient power; otherwise, it will be in charging mode.

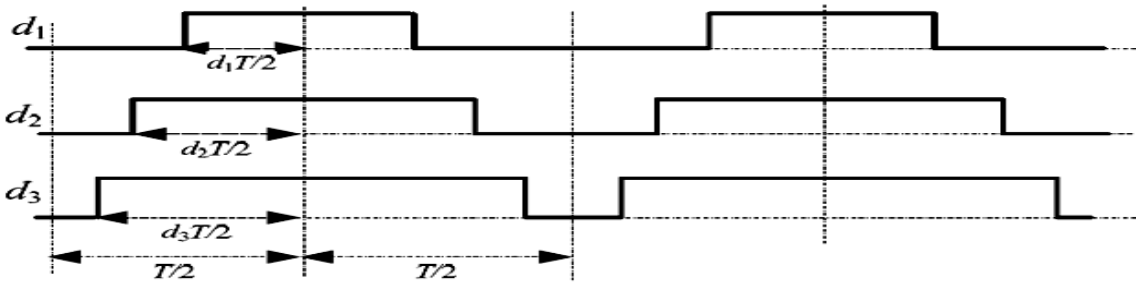

Fig. 10: Gate signal of the proposed APFC controller

Figure 10 Gate signal of the proposed APFC controller. The duty cycle is symmetric in regard to the half period, which means that the switching time of the kth switch is (1 - dk)T/2. Which is based on the source power stability; if all power generation has attained the stability generation, all switches are switched on at the same time.

E Voltage Source Inverter

The standard three-phase voltage source is given in the inverter, and eight valid switches listed are in the table. The three-phase inverter circuit is shown in Figure 11, and the switching operations (Q1 and Q4, Q3 and Q6, or Q5 and Q2) are in Table 1. Similarly, in inverting states with no undefined output AC line voltages in VSI, the inverter can no longer turn off any switches simultaneously. It cannot cause the voltage to depend on the current line current polarity. There are eight active and two zero AC line voltage. In this case, the AC at the top or bottom of the flywheel.

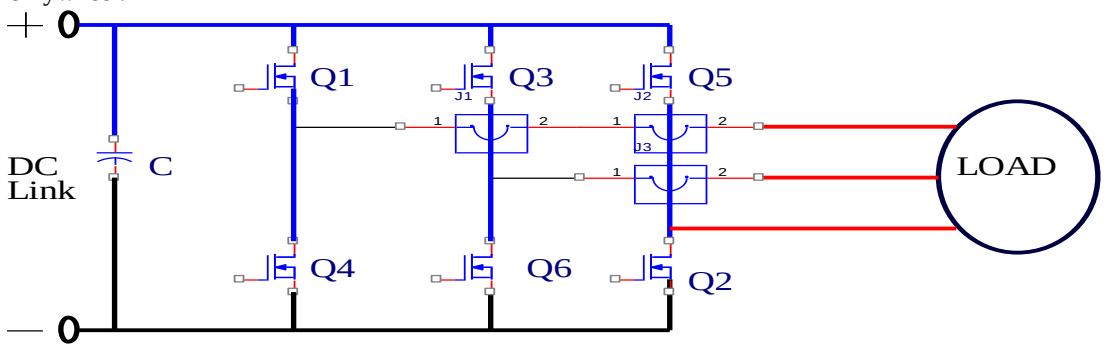

Fig. 11: Inverter circuit diagram

As a result, the output voltages V_i, 0, have voltage values of voltages, such as $-V_i$. The modulating technique is made to confirm that states only choose valid conditions to create a given waveform.

Table. 1: Inverter Switching State

ON State	OFF State	Switching Frequency	V_{ab}	V_{bc}	V_{ca}
Q1,Q2 and Q6	Q4,Q5 and Q3	5Khz	V_t	0	$-V_t$
Q2,Q3 and Q1	Q5,Q6 and Q4	5Khz	0	V_t	$-V_t$
Q3,Q4 and Q2	Q6,Q1 and Q5	5Khz	$-V_t$	V_t	0
Q4,Q5 and Q3	Q1,Q2 and Q6	5Khz	$-V_t$	0	V_t
Q5,Q6 and Q4	Q2,Q3 and Q1	5Khz	0	$-V_t$	V_t
Q6,Q1 and Q5	Q3,Q4 and Q2	5Khz	V_t	$-V_t$	0
Q1,Q3 and Q5	Q4,Q6 and Q2	5Khz	0	0	0
Q4,Q6 and Q2	Q1,Q3 and Q5	5Khz	0	0	0

The current non-zero output condition of the AC voltage. The switching action generates a sinusoidal output. When the switches are actuated, six different forms of switching circumstances are used to create the output voltage from the inverter. Phase matching is achieved using a microcircuit reference or input signal. The voltage of the carrier amplitude is less than that of the input message.

APFC Algorithm Steps

The steps for designing a Grid-tie Solar, Wind and Fuel cell Energy stability System. The Assimilate Power Flow Control (APFC) technique approach presented here is logical, and a step-by-step procedure is given below.

Step 1: Find the collected data from the renewable energy source (solar, Wind and battery system) that are input.

Step 2: The hybrid system models and records the data obtained and the threshold value to find a plurality of predictive linear model.

Step 3: An objective function of the system is to absorb the RES's MPPT data and vary the MPC's PWM.

Step 4: Energy demand stabilization

$$P_{Load}(t) = PV_{power}(t) + P_{WG}(t) \quad \ldots \quad (22)$$

Upper and lower limits generation bound are given below;

$$\overline{P}_n \leq \underline{P}_n(t) \leq \overline{P}_n \quad \ldots \quad (23)$$

Where,

$P_{Load}(t)$ = load

$PV_{power}(t)$ = PV output power

$P_{WG}(t)$ = Wind output

$\overline{P}_n$ *and* $\underline{P}_n$ = upper and lower generation bound.

Step 5: For the new set of periodical data at time t, the predicted solar intensity and wind power are obtained from the correction.

Step 6: Find the errors from two systems and go to the next step.

$$\epsilon l(t) = |v(t) - y(t)| \quad \ldots \quad (24)$$

$$\epsilon h(t) = |v(t) - y(t)| \quad \ldots \quad (25)$$

Step 6: During the(V)) and ϵh(t) , the APFC controller will vary the pulse of the converter and inverter.

Step 7: Duty cycle d is a crucial control variable for the overall produced power system's implementation of automated control and balancing power under varied operating situations.

Step 8: Otherwise, the battery continually charges with the rapidly monitoring charge control circuit.

Restore the initial value of I bat, max (26)

Step 9: Adjust the duty cycle D=$\alpha, \alpha+1, \alpha+2, \alpha+3, \ldots\ldots \alpha+N$ to the DC-DC converter when the HRES is fluctuating.

Step 10 when the load system and multi-power generation are equal: they maintain the D=α; go to step 6

Step 11: Balance of power supply and demand from the grid is

$$P_{grid}(t) = P_{LD}(t) - P_{PV}(t) - P_{WG}(t) \quad \ldots \quad (27)$$

Step 12: Keep the unchanged data, recurrence from step 3 until all new data are managed.

Step 13: Stop.

IV. RESULTS AND DISCUSSION

A Simulation Result

Modelling method of a Mat lab-based toolset for building and testing a multiport DC-DC converter based on the Assimilate Power Flow Control (APFC) technique under different operational situations. The proposed novel APFC model is developed in a mat lab setting. The renewable energy management system generates the system's energy power source using a distinct power-generating method. A converter will control insufficient energy sources, resulting in higher voltage on the source side. The system power control algorithm is required for power management, and the APFC controller is employed for improvement.

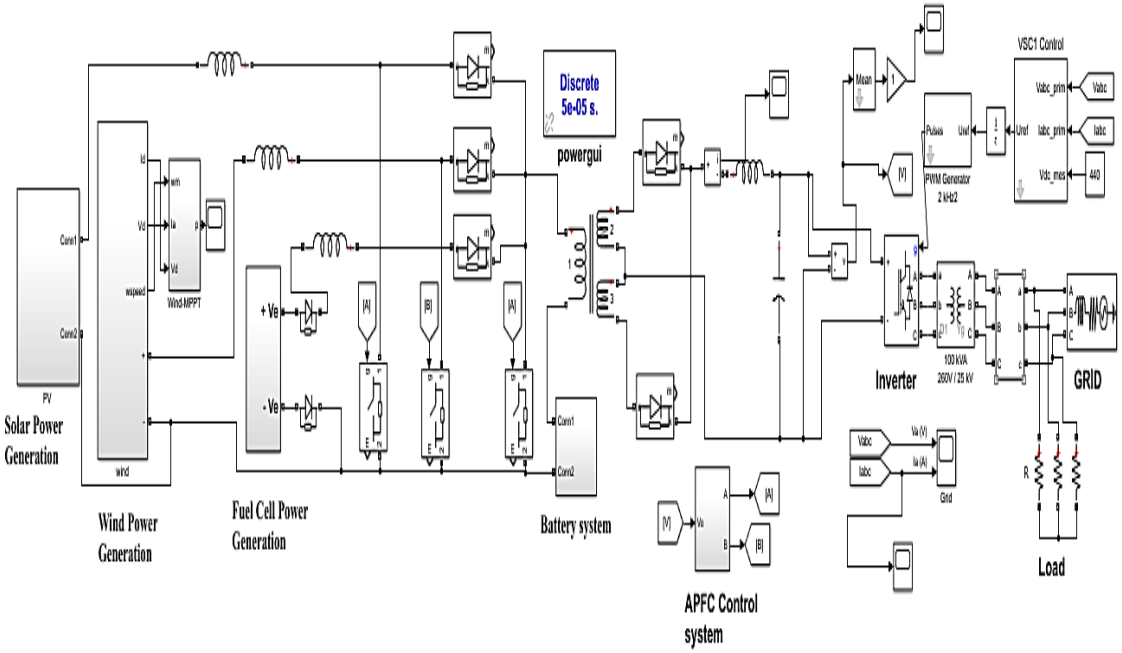

Fig. 12: Proposed Simulink Model

Figure 12 represents the proposed MPC; in this system, three different energy sources are utilized: Solar, Wind and fuel cell-based energy generation. Battery-based energy management is also implemented to ensure continuous and stable energy flow in the DC bus system. Finally, the inverter can convert the stabilized DC voltage into AC. Using the Assimilate Power Flow Control (APFC) technique will improve power quality, the results of which are described below.

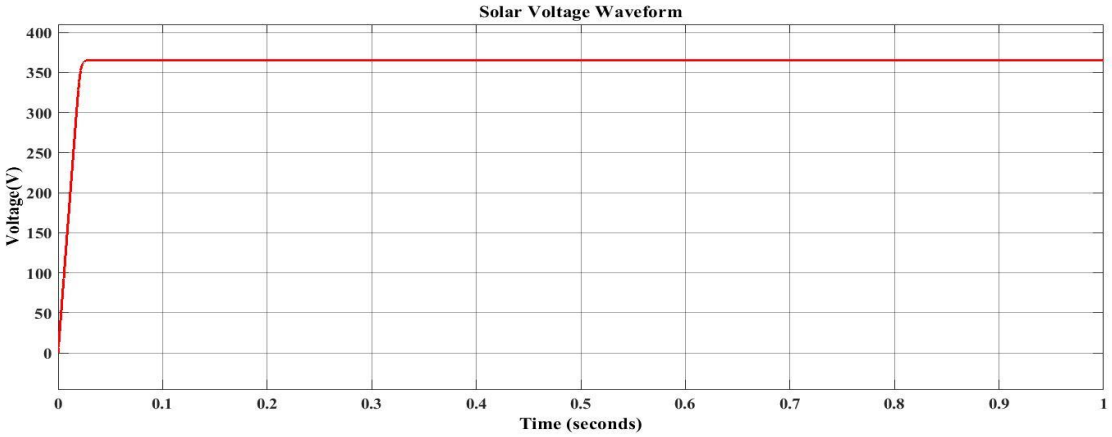

Fig. 13: Solar output power

Figure 13 displays the solar generation waveform based on the above waveform, and it clearly illustrates the 300 V on the y-axis in terms of seconds.

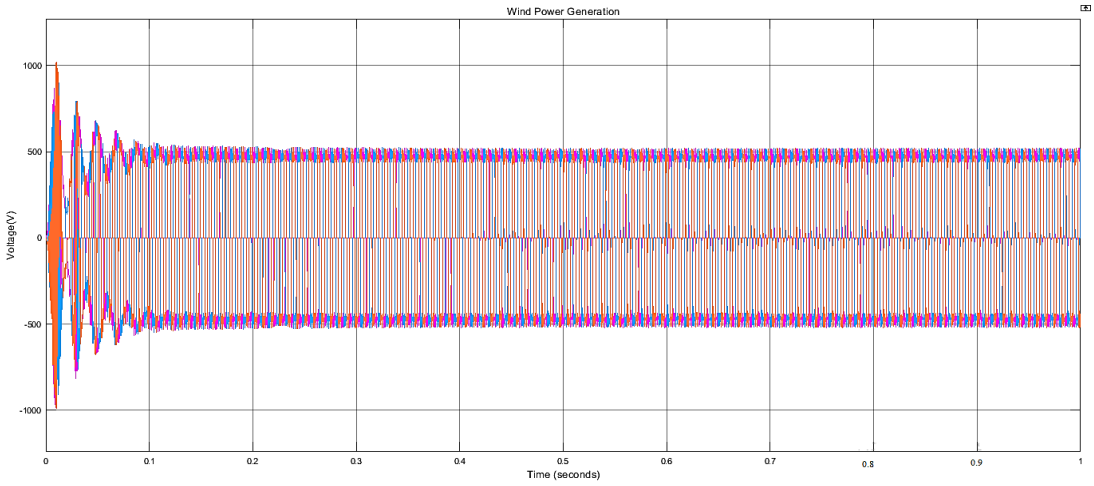

Fig. 14: Wind voltage waveform

The energy output was applied to the maximum power wind sample with the acquired voltage of 500 V at time t = 1s, as indicated in Figure 14.

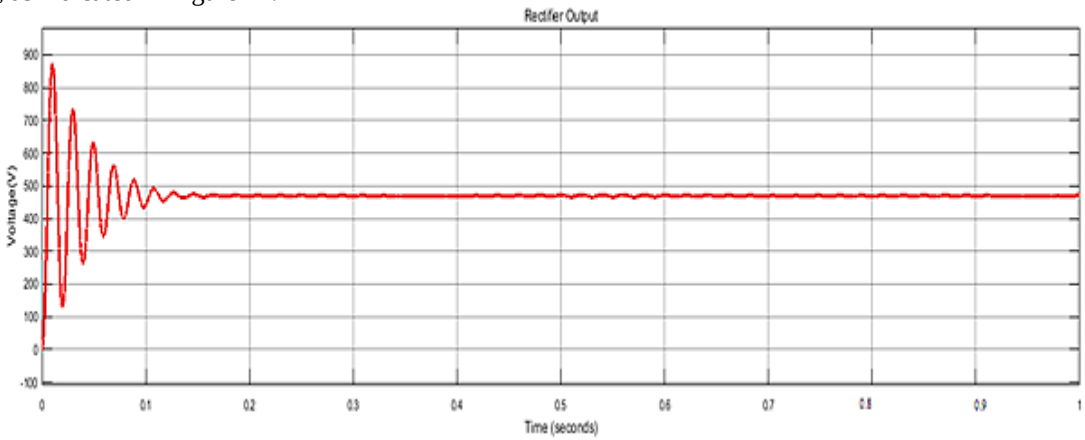

Fig. 15: Wind Energy stabilization waveform

MPC will maintain the production of wind energy. A rectifier is used for AC to DC conversion as a result of this procedure. The rectified DC voltage of the wind energy generation employed as the MPC input source is shown in Figure 15. This indicates the voltage on the y-axis; the time t = 1 second is shown on the x-axis in V = 450 constant voltage.

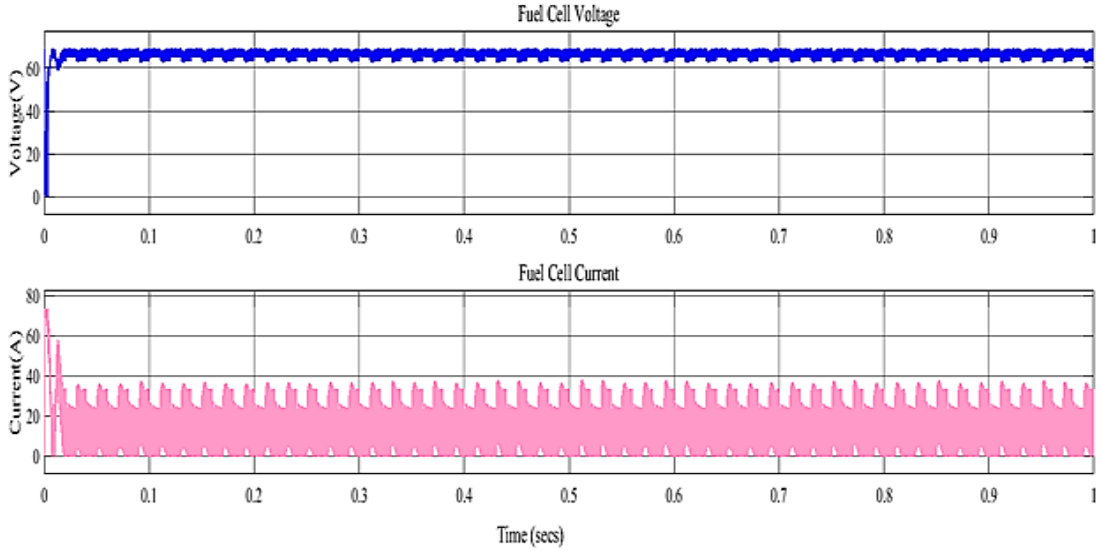

Fig. 16: Fuel Cell Generation Waveform

Fuel cell production depends on combined voltage and current waveforms, as seen in Figure 16. The fuel cell generates 65 V of voltage, as shown in the seconds in the above picture. The voltage determines the current value of 22 A concerning time in seconds.

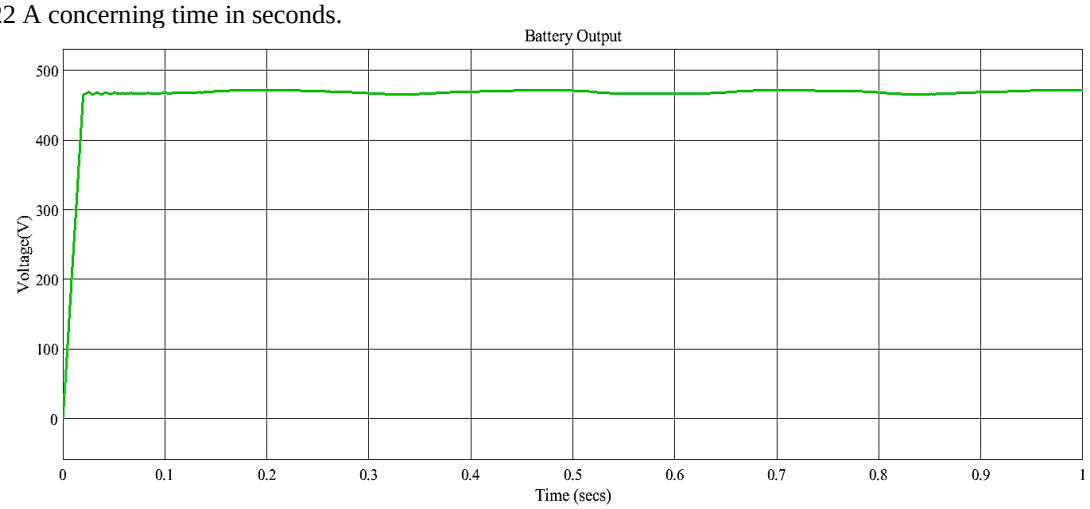

Fig. 17: Battery Output

By taking advantage of the battery system, the suggested MPC system continuously generates power for the bus system. There are two ways to use the battery-based energy management system: charging and discharging. The charging mode waveform of the battery system is depicted in Figure 17, where the battery voltage is 440 V on the y-axis for a length of 1s.

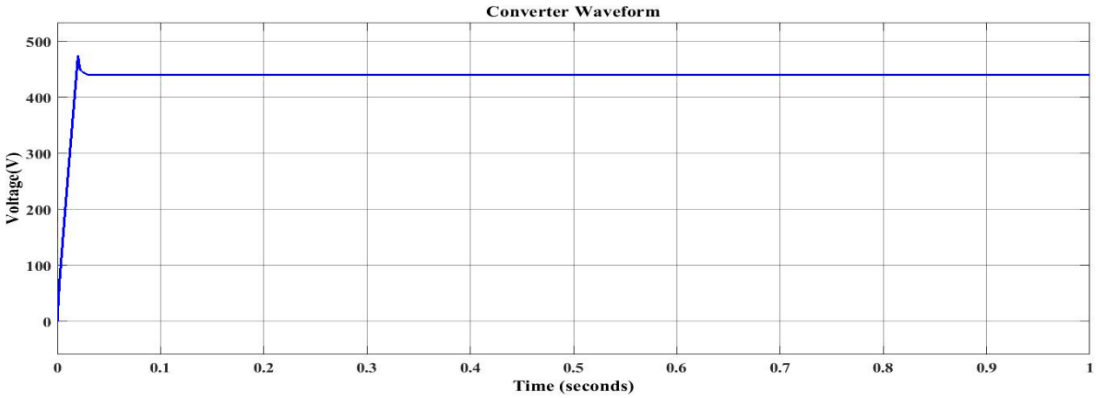

Fig. 18: Multiport converter output

The MPC voltage from many input sources, including fuel cells, voltage, and solar power, is depicted in Figure 18. Nevertheless, each energy source generates a distinct voltage level, as seen in Figures 12, 14, and 15. The purpose of the multiport converter is to regulate the DC voltage. The stable 440 V DC system is displayed in Figure 14, with the time interval expressed in seconds.

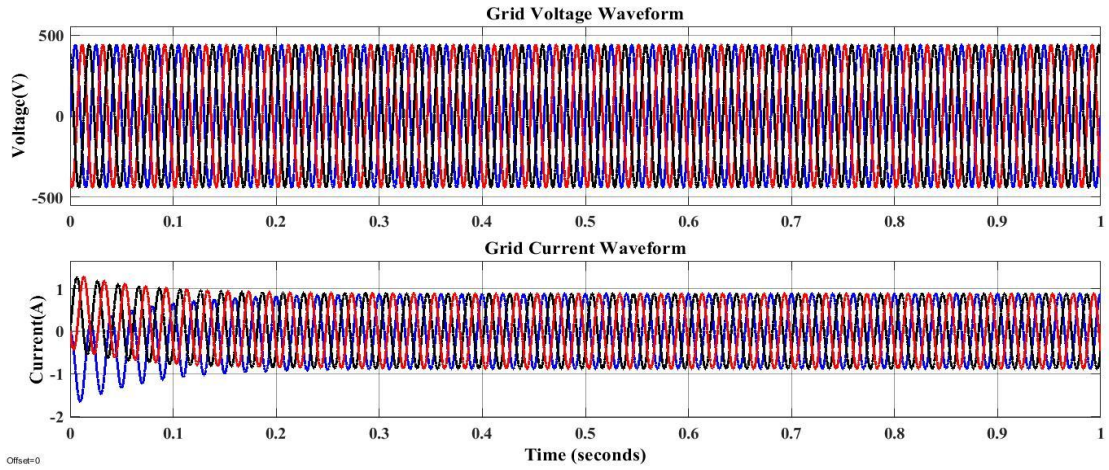

Fig. 19: Grid power waveform

Figure 19 displays the power of the present grid and the ideal grid voltage. The x-axis shows the duration T = 1s, while the y-axis depicts the phase supply voltage, 4400 V. The load indicates that the x-axis represents T = 1 s, and the waveform's current display is shown on the y-axis = 4A.

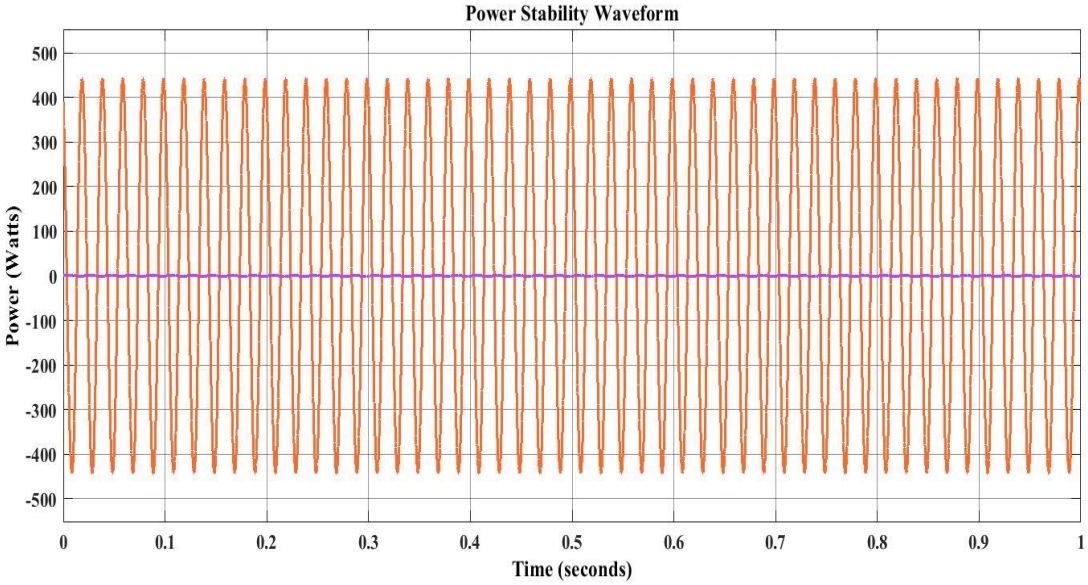

Fig. 20: Load current and Voltage waveform.

Figure 20 The relative differential periods represent the load voltage waveforms and current. The waveform attests to the nearly uniform power stability under all load conditions.

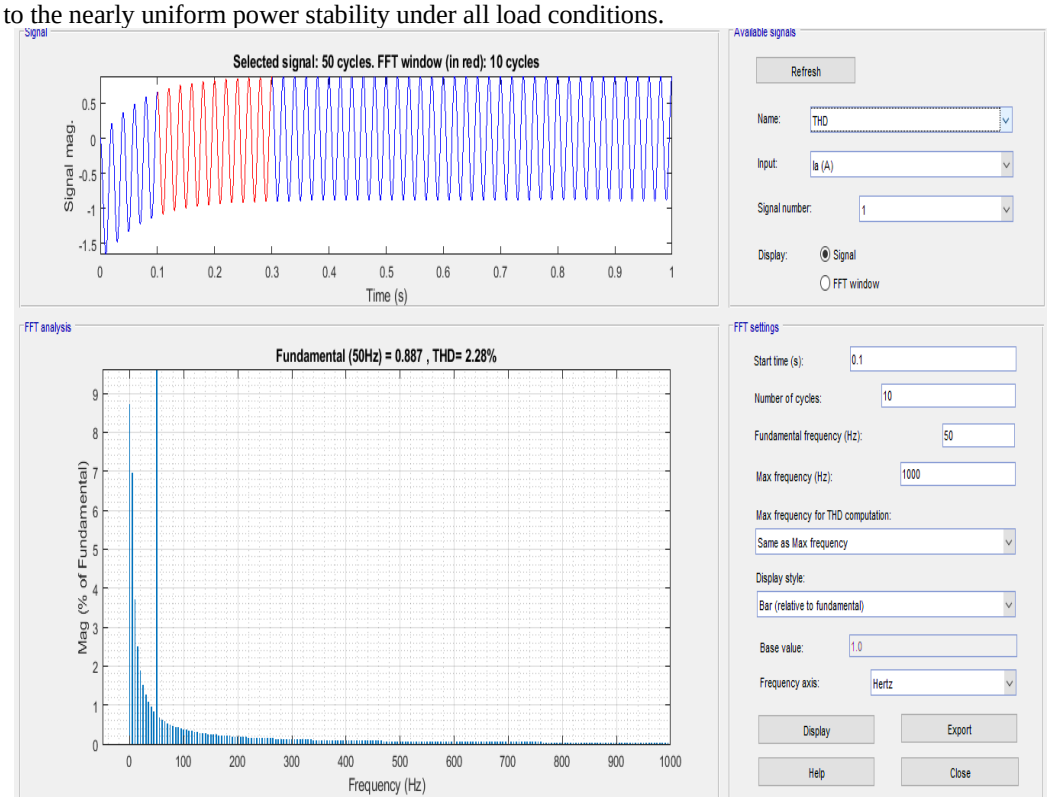

Fig. 21: THD analysis

Figure 21 represents the THD study for the proposed MPC system waveform with the APFC control method, yielding 2.28%.

B Experimental Result

The proposed solution uses an experimental configuration with non-isolated converters that operate in grid-connected output mode. The centralized converter monitors the operational voltage of photovoltaic, Wind, and Fuel Cell renewable power sources and the battery management system. If the operational voltage of the photovoltaic system exceeds the demand and the fuel cell cannot meet the requirements, the photovoltaic system

is planned to supply the load while the fuel cell remains inactive, and vice versa. Both providers work concurrently if they can each separately happen to meet the load but their combined production is enough to cover it. However, having a backup plan in place becomes essential if the combined production of both sources is inadequate to fulfil the demand.

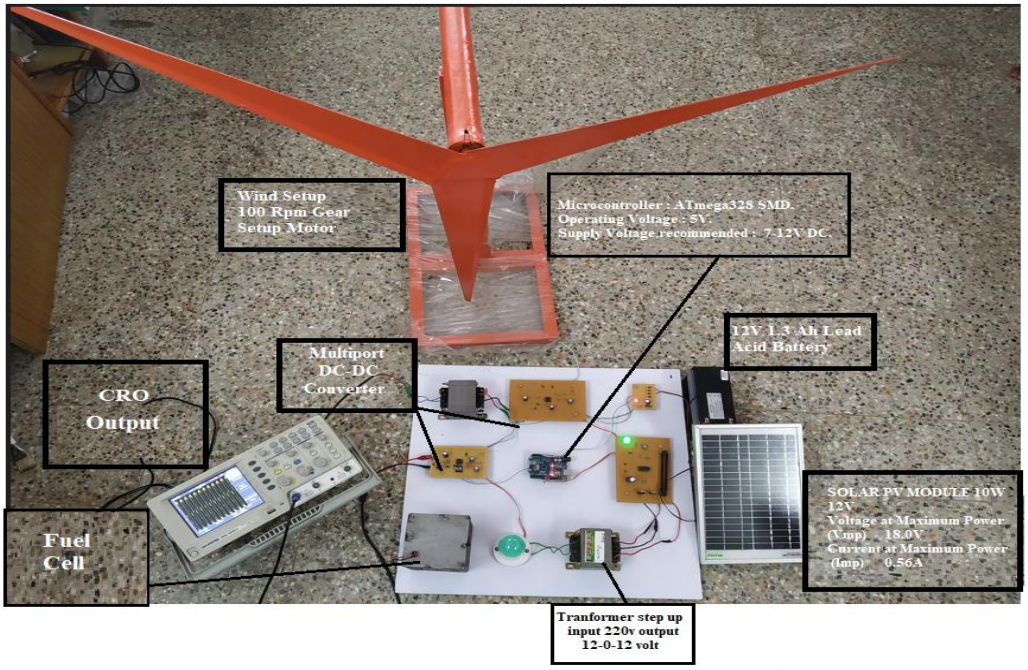

Fig. 22: Hardware output of proposed hardware output

Figure 22 shows the hardware consists of an input source of the photovoltaic, Wind, and Fuel cells interconnected with an Isolated Multiport DC-DC Converter. The photovoltaic panel generates a DC input source, the Wind produces an AC input source, and the fuel cell creates a DC input source. The is connected to a multiport is connected with multiport DC-DC Converter is controlled with an Assimilate Power Flow Control algorithm-controller technique; the PWM pulse to the switching device is regulated based on each mode of operation conducted in the multiport converter; the inverter initially DC-AC supply and output load voltage, and each mode varies with different voltage based on load demand.

In the experimental results presented below, a prototype was established to examine the validity and accuracy of the proposed Isolated Multiport DC-DC Converter and Assimilate Power Flow Control algorithm. The prototype includes power and control boards, as well as the switch driver, with units connected to the output of the converter.

Hardware output gain of the DSO:

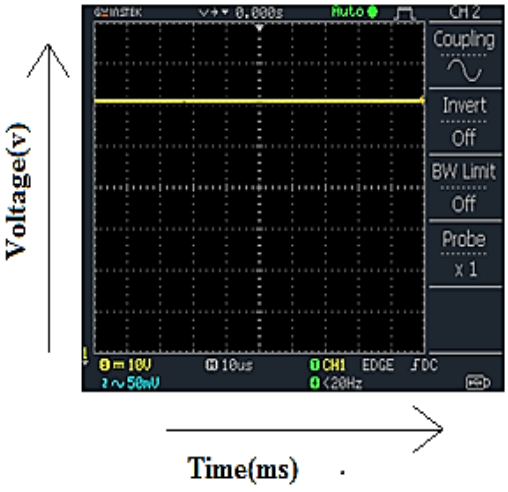

Fig. 23: Battery output voltage

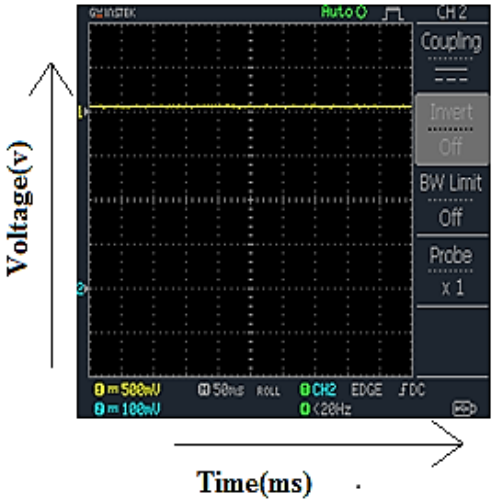

Fig. 24: DC-DC converter output

The battery output voltage of the renewable energy system, which seems to gain 10Vo DC power, is shown in Figure 23. Figure 24 illustrates the boost converter voltage that is supplied by the battery power. The converter's output surpasses 24V DC in comparison to the battery voltage.

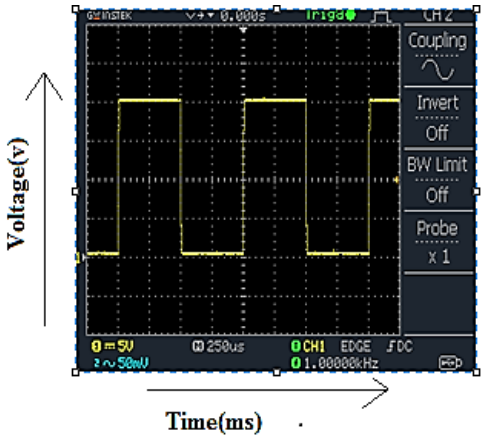

Fig. 25:(A) PWM Form the Microcontroller

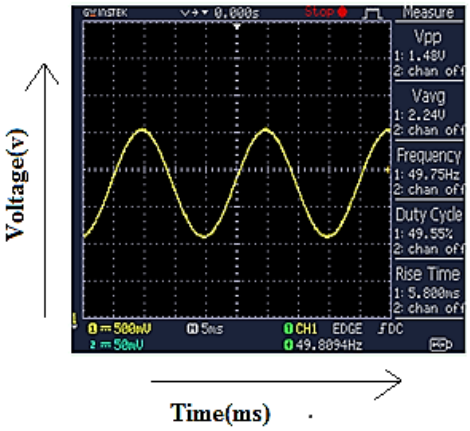

Fig. 25: (B) Inverter output.

The PWM voltage is sent to the inverter to convert the voltage variability, as shown in Figure 25 (A). The waveform indicates a PWM voltage of 5VDC, and the hybrid method's converter is obtained, which means the voltage value is V=230V AC. Figure 25 (B) displays the inverter gain for the hybrid method with a connected load power gain, and it denotes the voltage value V=230V AC.

C Simulation and Experimental Calculation

Table. 2: Analysis of the performance of the MPC system using various loads

Methods	Steady-state error (%)	THD (%)	Execution time(sec)	Efficiency (%)
PID	0.594	6.9	0.7864	89.32
APFC	0.326	2.28	0.3120	93.86

Table 2 demonstrates the Performance analysis of the MPC system based on various control strategy systems based on parameters like THD (%), Execution time (sec), Steady-state error (%), and efficiency in (%).An improved outcome is obtained when the suggested APFC control approach is compared with all of the previously mentioned factors.

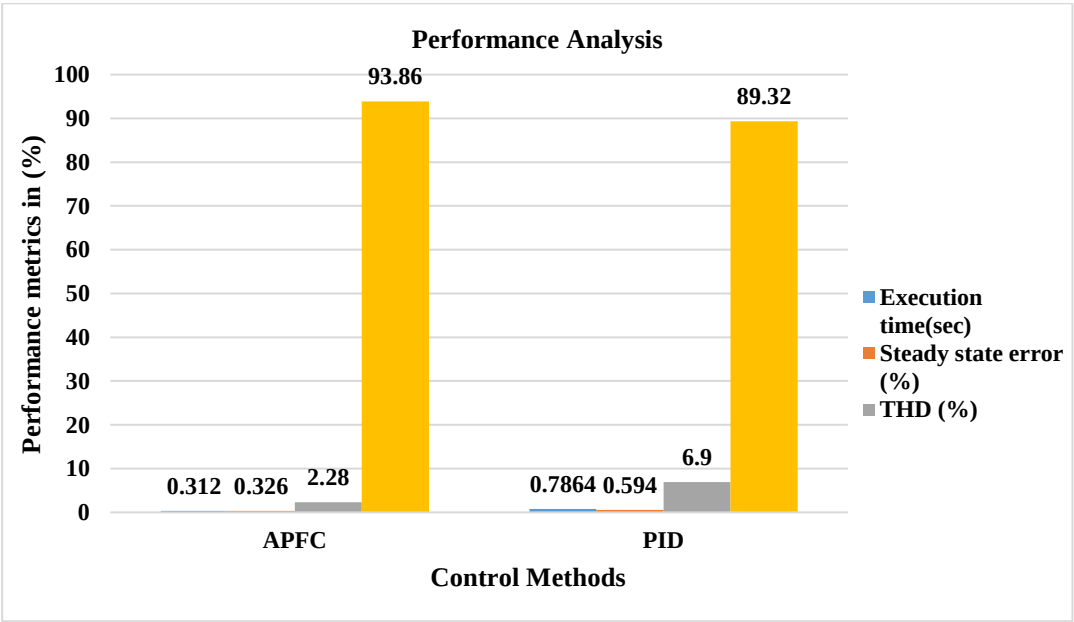

Fig. 25: Performance analysis

Figure 25 shows the MPC system performance analysis; from the proposed research, Assimilate Power Flow Control (APFC) produced a better result than the Proportional Integral Derivative (PID) controller.

Table. 3: Performance examination of power factor for varied loads

Controller	Voltage(V)	Current(A)	Load (W)
APFC	440	1.2	500
	440	2.27	1000
	440	3.2	1500

Table. 3 explains the performance study of the suggested system load stability under various load circumstances.

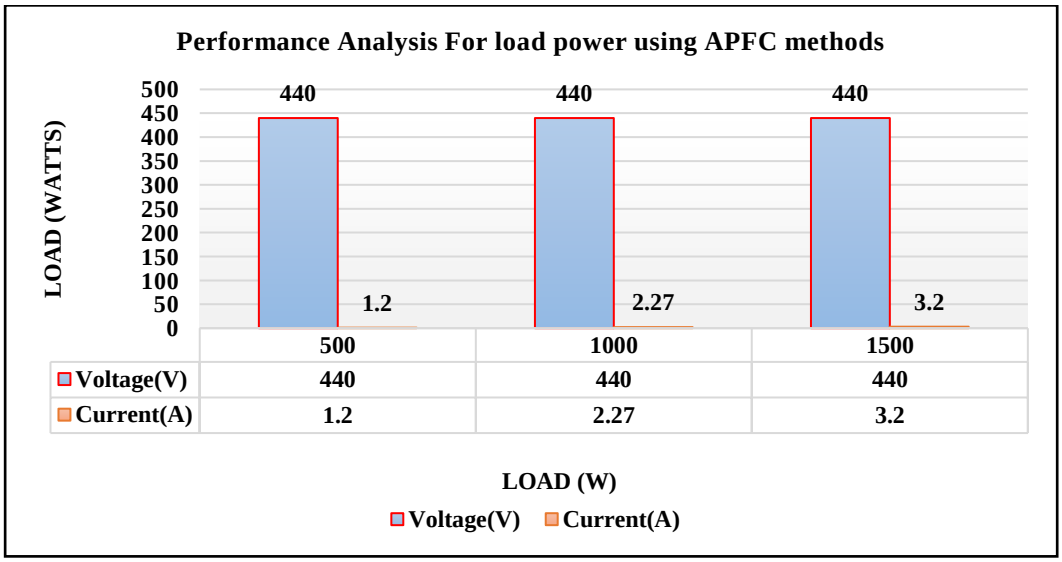

Fig. 26: Performance proposed model in settings when the load varies.

The performance study of the proposed model with changing loads is displayed in Figure 26. Under load-varying (0-1500) issues, the suggested Assimilate Power Flow Control (APFC) Controller will yield efficient outcomes.

Efficiency Formula:

$$\text{Efficiency} = \frac{\text{Maximum Possible output}}{\text{Actual Input}} \text{X } 100\% \ldots \quad (28)$$

Actual input power=1500 W

Maximum possible output=440(V) x3.2 (A) =1408W

$$= \frac{1408}{1500} X 100\%$$

$$=0.9386 \times 100\%$$

Efficiency =93.86%.

V. CONCLUSION

This work analyses a newly implemented multiport converter topology using a renewable energy system. This freshly implemented multiport DC-DC converter system has different renewable energy sources like solar, wind, and fuel cells; the proposed converter system's additional benefit is battery-based energy management. For input source stabilization purposes in the MPC, an advanced control technique called Assimilate Power Flow Control (APFC) is utilized to switch the MPC appropriately. The switching activity of the MPC will stabilize the input source with a high steady state condition. In hardware porotype shows the output voltage (V) from the inverter Measured on CRO, and the performance of the proposed Assimilate Power Flow Control (APFC) control techniques is examined using several criteria like steady-state error 0.326 (%), THD (2.28%) and efficiency (93.86%) from simulation.

REFERENCE

[1] Aravind. R, B. Chokkalingam and L. Mihet-Popa, "A Transformerless Non-Isolated Multiport DC–DC converter for hybrid energy applications", IEEE Access, vol. 11, pp. 52050-52065, 2023.

[2] B. N. Alajmi, M. I. Marei and I. Abdelsalam, “A Multiport DC-DC Converter Based on Two-Quadrant Inverter Topology for PV Systems”, IEEE Transactions on Power Electronics, vol. 36, no. 1, pp. 522-532, 2021.

[3] Bahravar. S, Abbaszadeh. K and Olamaei, J, “High Step-Up Non-isolated DC–DC Converter Using Diode–Capacitor Cells”, Iranian Journal of Science and Technology, Transactions of Electrical Engineering, pp. 45, 81–96, 2021.
[4] Chandrasekar. B, et al, “Non-isolated high-gain triple port DC–DC buck-boost converter with positive output voltage for photovoltaic applications”, IEEE Access, vol. 8, pp. 113649-113666, 2020.
[5] Chandrasekar. Bet al., “Non-Isolated High-Gain Triple Port DC-DC Buck-Boost converter with positive output voltage for photovoltaic applications”, IEEE Access, vol. 8, pp. 113649-113666, 2020.
[6] Chaudhury. T and D. Kastha, "A High Gain Multiport DC-DC Converter for Integrating Energy Storage Devices to DC Microgrid", IEEE Transactions On Power Electronics, vol. 35, no. 10, pp. 10501-10514, 2020.
[7] Chen. G, Y. Liu, X. Qing and F. Wang, “Synthesis of integrated multiport DC-DC converters with reduced switches”, IEEE Transactions on Industrial Electronics, vol. 67, no. 6, pp. 4536-4546, 2020.
[8] Faraji. Rand H. Farzanehfard, "Fully soft-switched Multiport DC-DC converter with high integration", IEEE Transactions on Power Electronics, vol. 36, no. 2, pp. 1901-1908, 2021.
[9] Filsoof. K and P. W. Lehn, “A Bidirectional Multiple-Input Multiple-Output Modular Multilevel DC-DC Converter and its Control Design”, IEEE Transactions on Power Electronics, vol. 31, no. 4, pp. 2767-2779, 2016.
[10] Ganjavi. A, H. Ghoreishy and A. A. Ahmad, “A Novel single-input dual-output three-level DC-DC converter”, IEEE Transactions on Industrial Electronics, vol. 65, no. 10, pp. 8101-8111, 2018.
[11] Hoffmann. F, J. Lafrenz, M. Liserre and N. Vazquez, “Isolated Multiport Converter as Cost-Efficient Solution for DC-Fast Charger of Electric Vehicle,” IECON - 45th Annual Conference of the IEEE Industrial Electronics Society, Lisbon, Portugal, pp. 4905-4910, 2019.
[12] Jalilzadeh. T, N. Rostami, E. Babaei and S. H. Hosseini, “Multiport DC-DC converter with step-up capability and reduced voltage stress on Switches/Diodes”, IEEE Transactions on Power Electronics, vol. 35, no. 11, pp. 11902-11915, 2020.
[13] Kougioulis. I, A. Pal, P. Wheeler and M. R. Ahmed, “An Isolated Multiport DC–DC converter for integrated electric vehicle on-board charger”, IEEE Journal of Emerging and Selected Topics in Power Electronics, vol. 11, no. 4, pp. 4178-4198, 2023.
[14] Kung S. H and G. J. Kish, “Multiport modular multilevel converter for DC systems”, IEEE Transactions on Power Delivery, vol. 34, no. 1, pp. 73-83, 2019.
[15] M. Jafari, Z. Malekjamshidi, D. D. -C. Lu and J. Zhu, “Development of a Fuzzy-logic-based energy management system for a multiport multi-operation mode residential smart Micro-grid”, IEEE Transactions on Power Electronics, vol. 34, no. 4, pp. 3283-3301, 2019.
[16] Qin. F, T. Hao, F. Gao, T. Xu, D. Niu and Z. Ma, “A Multiport DC-DC Modular Multilevel Converter for HVDC Interconnection”, IEEE Applied Power Electronics Conference and Exposition (APEC), New Orleans, LA, USA, pp. 520-524, 2020.
[17] Sato. Y, M. Uno and H. Nagata, “Non-isolated Multiport Converters Based on Integration of PWM Converter and Phase-Shift-Switched Capacitor Converter”, IEEE Transactions on Power Electronics, vol. 35, no. 1, pp. 455-470, 2020.
[18] St-Onge X. F, C. Richard, K. M. McDonald and S. S. A. Saleh, "Performance Testing of an Active Multiport DC Link for Grid-Connected PMG-Based WECSs", IEEE Transactions On Industry Applications, vol. 54, no. 6, pp. 5579-5589, 2018.
[19] Subramanian. Karuppiah, S, “Analysis of dual-input three-port isolated DC–DC converter with bidirectional capability”, Journal of Power Electronics, pp. 711–726, 2022.
[20] Uno. M and K. Sugiyama, “Switched-capacitor converter based Multiport converter integrating bidirectional PWM and series-resonant converters for standalone photovoltaic systems”, IEEE Transactions on Power Electronics, vol. 34, no. 2, pp. 1394-1406, 2019.
[21] Varesi. K, S. Hossein Hosseini, M. Sabahi, E. Babaei, S. Saeidabadi and N. Vosoughi, “Design and analysis of a developed multiport high step-up DC-DC converter with reduced device count and normalized peak inverse voltage on the Switches/Diodes”, IEEE Transactions on Power Electronics, vol. 34, no. 6, pp. 5464-5475, 2019.
[22] Wang. B et al., "Consensus-based control of hybrid energy storage system with a cascaded multiport converter in DC microgrids", IEEE Transactions on Sustainable Energy, vol. 11, no. 4, pp. 2356-2366, 2020.
[23] Wu. H, L. Zhu and F. Yang, “Three-Port-Converter-based single-phase bidirectional AC–DC Converter With Reduced Power Processing Stages and improved overall efficiency”, IEEE Transactions on Power Electronics, vol. 33, no. 12, pp. 10021-10026, 2018.
[24] Zhao. S, Y. Chen, S. Cui, B. J. Mortimer and R. W. De Doncker, “Three-Port bidirectional operation scheme of modular-multilevel DC–DC converters interconnecting MVDC and LVDC Grids”, IEEE Transactions on Power Electronics, vol. 36, no. 7, pp. 7342-7348, 2021.
[25] Zhuang. F. Liu, X. Zhang, Y. Huang, X. Zha and Z. Liu, “Short-Circuit Fault-Tolerant Topology for Multiport Cascaded DC/DC Converter in Photovoltaic Power Generation System”, IEEE Transactions on Power Electronics, vol. 36, no. 1, pp. 549-561, 2021.
[26] A. K. Sahu, V. K. Chandra and G. R. Sinha, "High level computation technique for characterization of sigma-delta a/d converter," 2017 International conference on Microelectronic Devices, Circuits and Systems (ICMDCS), Vellore, India, 2017, pp. 1-4, doi: 10.1109/ICMDCS.2017.8211601.
[27] Dimlo, UM Fernandes, R. Umanesan, Jonnadula Narasimharao, N. Senthamilarasi, P. S. Ranjit, B. Balaji, I. Thamarai, and Vijay Kumar Dwivedi. "Optimal Configuration Planning of Multi-Energy Systems using Optimization-based Deep Learning Technique." *Electric Power Components and Systems* (2023): 1-16.

[28] Sudhamani Chilakala *, Saxena Ashutosh and Aswini Vunnava, Improved Detection Performance of Energy Detection Based Spectrum Sensing in Cognitive Radio Networks, International Journal of Sensors, Wireless Communications and Control 2021; 11 (9) . https://dx.doi.org/10.2174/2210327911666210219115009